THE JOURNAL OF PHYSICAL CHEMISTRY A

Article

pubs.acs.org/JPCA

Stability of Gas-Phase Tartaric Acid Anions Investigated by Quantum Chemistry, Mass Spectrometry, and Infrared Spectroscopy

Ralf Tonner,[†] Peter Schwerdtfeger,[†,‡] Amanda L. May,[§] Jeffrey D. Steill,[§,∥,▽] Giel Berden,[∥] Jos Oomens,[∥,⊥] Shawn R. Campagna,[§,*] and Robert N. Compton[§,¶,*]

[†]Fachbereich Chemie, Philipps-Universität Marburg, Hans-Meerwein-Straße, 35032 Marburg, Germany

[‡]The New Zealand Institute for Advanced Study (NZIAS), Massey University Albany, Private Bag 102904, North Shore MSC, Auckland, New Zealand

[§]Department of Chemistry, The University of Tennessee, Knoxville, Tennessee 37996, United States

[∥]FOM-Institute for Plasma Physics Rijnhuizen, Edisonbaan 14, 3439 MN Nieuwegein, The Netherlands

[⊥]Van't Hoff Institute for Molecular Sciences, University of Amsterdam, Science Park 904, 1098 XH Amsterdam, The Netherlands

[¶]Department of Physics, The University of Tennessee, Knoxville, Tennessee 37996, United States

Supporting Information

ABSTRACT: In an effort to understand the chemical factors that stabilize dianions, experimental and theoretical studies on the stability of the tartrate dianion were performed. Quantum chemical calculations at the coupled cluster level reveal only a metastable state with a possible decomposition pathway $(O_2C-CH(OH)-CH(OH)-CO_2)^{2-} \rightarrow (O_2C-CH(OH)-CH(OH))^{\bullet -} + CO_2 + e^-$ explaining the observed gas-phase instability of this dianion. Further theoretical data were collected for the bare dianion, this molecule complexed to water, sodium, and a proton, in both the meso and L forms as well as for the uncomplexed radical anion and neutral diradical. The calculations suggest that the L-tartrate dianion is more thermodynamically stable than the dianion of the meso stereoisomer and that either dianion can be further stabilized by association with a separate species that can help to balance the charge of the molecular complex. Mass spectrometry was then used to measure the energy needed to initiate collisionally induced dissociation of the racemic tartrate dianion and for the proton and sodium adducts of both the racemic and meso form of this molecule. Infrared action spectra of the dianion stereoisomers complexed with sodium were also acquired to determine the influence of the metal ion on the vibrations of the dianions and validate the computationally predicted structures. These experimental data support the theoretical conclusions and highlight the instability of the bare tartrate dianion. From the experimental work, it could also be concluded that the pathway leading to dissociation is under kinetic control because the sodium adduct of the racemic stereoisomer dissociated at lower collisional energy, although it was calculated to be more stable, and that decomposition proceeded via C–C bond dissociation as computationally predicted. Taken together, these data provide insight into the gas-phase stability of the tartrate dianion and highlight the role of adducts in stabilizing this species.

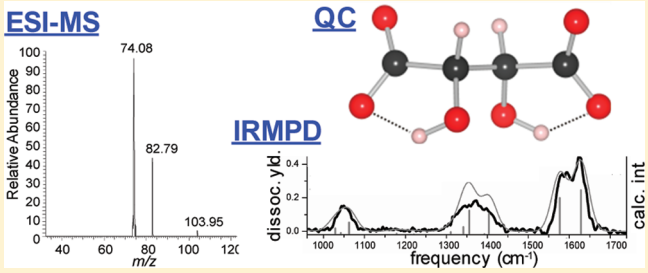

1. INTRODUCTION

The colorless and odorless tartaric acid compound exists as a translucent organic crystal, which can be found as a natural product in grapes, bananas, and many other plants.[1−3] Although tartaric acid is a muscle toxin (large amounts can lead to potential paralysis and death), many of its derivatives, such as potassium bitartrate (cream of tartar), are useful as food additives.[4] Tartaric acid has two stereocenters, and Pasteur's classic studies on the optical activity of both crystals and solutions of tartaric acid have played a central role in the development of modern stereochemistry.[5,6] The three tartaric acid isomers L (*R*, *R*), D (*S*, *S*), and meso (*R*, *S*) (Figure 1), have been well studied in organic chemistry and in biochemical processes such as tartaric acid metabolism.[7−9] Due to its desirable chemical properties and ready availability, tartaric acid is widely employed to aide in the synthesis and resolution of other chiral molecules.[10] Being highly soluble in water, tartaric acid exists as a singly or doubly charged anionic molecule depending upon the pH of the solution. In this study we examine the formation and structure of the gas-phase dianions, monoanions, and neutral diradicals of tartaric acid both experimentally and theoretically (Figure 2).

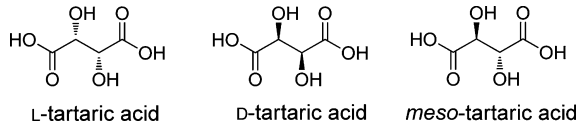

Figure 1. Stereoisomers of tartaric acid.

Received: January 20, 2012
Revised: April 8, 2012
Published: April 10, 2012

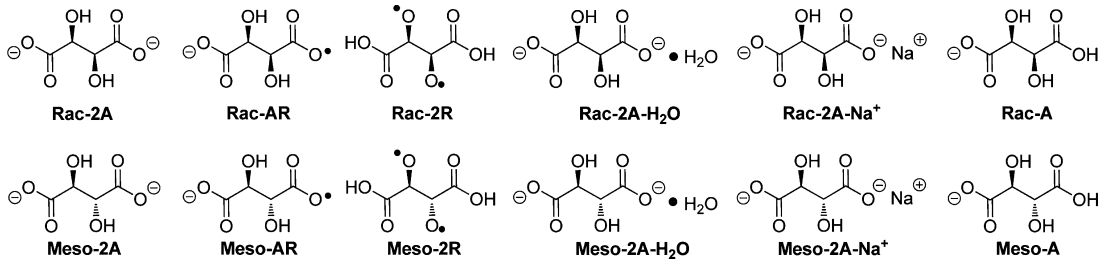

Figure 2. Various compounds investigated in this study. Note that only one enantiomer is shown for the racemic compound.

In addition, the stabilization of the tartaric acid dianion through counterion association and hydrogen bonding and the decomposition path toward dissociation are examined with regard to the Coulomb barrier to electron detachment and dissociation.

The stability of doubly negatively charged small molecules in the gas phase has long been of interest to chemists.[11] In the classical electrostatic model, two negative excess charges can be localized in a stable state at positions A and B in a molecule with corresponding electron-affinities E_A and E_B (defined as positive here) if the Coulomb repulsion between the two charges $E_C = e^2/4\pi\varepsilon_0 R_{AB}$ is less than E_A and E_B, i.e.,

$$\frac{e^2}{4\pi\varepsilon_0 R_{AB}} < \min\{E_A, E_B\} \quad \text{or} \quad \frac{4\pi\varepsilon_0}{e^2} R_{AB} \min\{E_A, E_B\} > 1 \tag{1}$$

As electron affinities are in the region of a few electronvolts, we obtain typical distances of $R_{AB} > 5$ Å. This distance between the two negative charges in tartaric acid is slightly longer at 6.5 Å. This simple electrostatic model rationalizes why there are no known doubly charged atoms or diatomics despite its usefulness to describe oxidation states,[12−16] and why it is so difficult to find small and compact molecules which can carry two negative charges.[17−19] Dianions can, however, be stabilized if the charges are delocalized, for example, by resonance stabilization as in the case of $[^-O—(CH{=}CH)_m—O^-]$ $(m \geq 10)$ and $[^-O—(C{\equiv}C)_k—O^-]$ $(k \geq 6)$.[20,21] However, Sommerfeld showed that aromatic stabilization in the dianions of cyclooctatetraene and cyclobutadiene is not sufficient to avoid electron loss.[22] The smallest known molecules calculated to be able to carry two negative charges are the metal halides MX_3^{2-} (M = Li, Na, X = F or Cl) and MX_4^{2-} (M = Be, Mg, Ca, X = F or Cl) predicted by Cederbaum and co-workers.[23−25] Some of these species have already been identified by experiment.[26] In some cases the dianion can exist in a long-lived metastable state in which electron decay occurs via tunneling through the Coulombic barrier. The best-known example is C_{60}^{2-}.[14,27,28]

Dicarboxylate dianions are well-known candidates for stabilizing two excess negative charges. Experiments and computational work confirm that acetylenedicarboxylate, $(O_2C—C{\equiv}C—CO_2)^{2-}$ is stable with respect to electron loss,[29,30] whereas the succinate dianion $(O_2C{-}CH_2{-}CH_2{-}CO_2)^{2-}$ is not. We hypothesize that this is both a distance and an electronic effect. The more rigid structure of the acetylene dicarboxylate creates a larger separation of charge, and the extended π system also allows delocalization of the negative charge. This electronic contribution from the slightly more electronegative sp-hybridized C should not be ignored,[30−32] and it should also be noted that strong electron withdrawing groups, such as fluorine, can help to stabilize such dianions as well.[21] We have also recently shown that the fumarate dianion, *trans*-$(O_2C—CH{=}CH—CO_2)^{2-}$, is Coulomb stable with respect to electron loss whereas maleate, i.e., the cis-isomer, is not; and these observations also support our distance hypotheses.[21] To further support these observations, the range of distances, which account for rotation about σ bonds, separating the dianions for the molecules above were measured from energy minimized structures, and it was found that two negative charges could be held between 5.5−5.9, 4.8−5.7, 2.5−5.7, and 1.5−6.1 Å apart from acetylenedicarboxylate, the fumarate dianion, the maleate dianion, and the succinate dianion, respectively. Ortho, meta, and para forms of aromatic dicarboxylate dianions derived from phthalic acids, $(O_2C—C_6H_4—CO_2)^{2-}$ have also been previously studied.[21,33] Quantum chemical investigations revealed that the para compound is the most stable and the ortho the least stable, in good agreement with the spatial negative charge separation.[21]

Another possible means to stabilize negative charges and thus avoid electron loss or fragmentation (in particular for organic molecules)[34,35] is by intramolecular hydrogen bridging. In this study we return to the problem of stabilizing the succinate dianion, $(O_2C—CH_2—CH_2—CO_2)^{2-}$, by introducing two hydroxyl groups to the carbon frame; i.e., we investigate anionic forms of tartaric acid $(O_2C—CH(OH)—CH(OH)—CO_2)^{2-}$. The initial question was to determine whether internal hydrogen bridging is sufficient to stabilize the doubly charged system with respect to electron loss or fragmentation, and if not, to identify factors that will stabilize this species. Further, it is to be expected that complexation with species capable of mediating electron density, e.g., a proton or sodium cation, will impart significant stability to the gas-phase tartrate dianion, thus comparison of the bare dianion to the dianion−Na^+ complex can give insight into the stability of the complex. The monoanion of tartaric acid can also provide some measure of the relative stability (or lack thereof) of this nonaromatic dicarboxylate dianion. Mass spectrometric and spectroscopic experimental investigations of the monoanion, dianion, and complexes were therefore undertaken to provide corroboration of the computational investigations.

2. COMPUTATIONAL AND EXPERIMENTAL METHODS

Computational studies of the tartrate dianion, monoanion and neutral diradical and its complexes are described herein. For every dianionic isomer of both diastereomers of tartaric acid (exemplified in Figure 2), a conformer search was conducted using the universal force field (UFF) as implemented in Avogadro0.9.[36] For the ten lowest-lying conformers, optimization without symmetry constraints was carried out using the Gaussian03[37] optimizer[38] together with TurboMole6[39] energies and gradients at the second-order Møller−Plesset (MP2) level of theory using def2-SVP basis sets.[40] All distinguishable conformers from this step were further optimized with the Dunning's correlation consistent aug-cc-pVTZ basis sets.[41,42] Characterization

dx.doi.org/10.1021/jp3007156 | J. Phys. Chem. A 2012, 116, 4789−4800

of stationary points has been achieved by numerically calculating the Hessian matrix for the best conformers and their transition states at the MP2/aug-cc-pVTZ level of theory as implemented in TurboMole6. For the decomposition path into CO_2 and the remaining fragment, the scan of the bond-breaking C−C bond lengths have been carried out by fully optimizing the structure under the condition of keeping the targeted bond length constant (relaxed scan). Additional energies have been derived using the MP2/aug-cc-pVTZ geometries at the MP2/aug-cc-pVDZ[43] and MP2/aug-cc-pVQZ[43] levels of theory to estimate the complete basis set limit (CBS)[44] using the procedure as outlined in ref 43. Further improved energies were calculated at the UCCSD(T)-F12[43]/cc-pVDZ-F12[45] level of theory using the program package Molpro2009.1.[46] Vertical electron detachment energies (VEDE) were calculated as the energy difference between the total energies of the monoanion (as single-point calculation on the optimized dianionic structure) and the dianion. Adiabatic electron detachment energies (AEDE) employed the total energy of the optimized anion instead. All calculations were carried out using the techniques known as resolution of identity (RI)[47−49] or density fitting (DF),[50,51] respectively. Open-shell species where calculated with unrestricted MP2 (UMP2) calculations (TurboMole) based on unrestricted Hartree−Fock (UHF) wave functions, whereby the CCSD(T) calculations (Molpro) used ROHF-wave functions as a starting point. Representations of molecules were generated using the program Vesta[52] whereas spin densities were plotted using gOpenMol.[53] Harmonic frequencies (ω) and IR intensities (I) for the most stable dianion have been calculated at the MP2/aug-cc-pVTZ level of theory. The MP2-frequencies were corrected for anharmonicity to obtain the fundamental transition frequencies (ν) by taking the difference ω(B3LYP-harmonic) − ν(B3LYP-anharmonic) after reoptimizing the structures, and adding it to the more accurate harmonic MP2-frequencies including all coupling terms in the cubic and quartic normal mode force fields according to the method outlined by Barone and co-workers.[54] The perturbative approach as described in detail by Schaefer and co-workers[55] and as implemented in Gaussian03,[37] was used for calculating the fundamental transition frequencies.[56−58] Simulated IR spectra were obtained by a convolution of the computed spectra with a Gaussian line shape and a half-width of 20 cm^{-1}. A thermochemical analysis was carried out at the MP2 level of theory to investigate entropy effects for the dianion stability.

We also investigated the addition of H_2O to the tartrate dianion. To find the global and few energetically low lying local conformer minima, we started from 20 different geometries with different positions of the H_2O molecule relative to the tartrate dianion, and carried out unconstrained optimizations with B3LYP/aug-cc-pVTZ followed by subsequent MP2/aug-cc-pVTZ optimizations on the remaining distinguishable structures. Finally, we investigated the complexation of the tartrate dianion with the Na^+ cation. The Na^+ adduct has been optimized at the same level of theory as the water adduct and bare dianion.

Mass Spectrometry-Collisional Dissociation Thresholds. Two mass spectrometers were used to carry out the experimental studies of tartaric acid, and both utilized direct infusion into an electrospray ionization (ESI) source for sample introduction. The first instrument, a Thermo Electron DECA XP plus linear ion trap (LCQ) mass spectrometer, was used to detect the bare dianion of racemic tartaric acid. The sample was introduced via a syringe with a flow rate of 30 μL/min, and data were collected for 1 min in the negative ionization mode. The ionization voltage was set to 2.5 kV, the capillary voltage was set to −7.1 V, the capillary temperature was set to 160 °C, and the tube lens voltage was set to −60 V. For fragment analysis, the parent m/z was selected with an isolation width of 1 m/z and CID was performed using helium as the collision gas at various energies. The collection time for the trap was set to 8000 ms to observe the dianion.

The second instrument was a quadrupole-time-of-flight (QTOF) QStar Elite from Applied Biosystems. This MS was used to measure both the parent m/z and fragmentation patterns for the monoanion and the Na^+ complex of both the racemic and meso tartrate dianions in negative ionization mode. The samples were introduced via a syringe at 20 μL/min into a TurboSpray Ion Source, and data were collected for 30 s. The nebulizing, curtain, and collision gas were set to 32, 20, and 5 (arbitrary units), respectively. The "ions pray" voltage was set to −2700 V, and the temperature was kept at 100 °C throughout all experiments. The set of compound parameters consisting of the declustering potential, focusing potential, and second declustering potential were set to −48, −84, and −19 (arbitrary units), respectively. The parent m/z was selected, and the product ions resulting from CID with N_2 were recorded in all MS^2 experiments.

For all measurements, a 1 mM solution of tartaric acid in water was injected and tandem mass spectrometric (MS^2) data were collected as described above. The selected parent ions were fragmented by increasing the collision energy stepwise until the parent m/z was no longer observed. For experiments studying the sodium adduct, an equimolar amount of sodium hydroxide was added to the solution.

Analysis of the data was performed using the Xcaliber MS software package (Thermo Electron). Data from the LCQ was imported directly to Xcaliber and processed using the Qual Browser application. Data from the QTOF required conversion from .WIFF format to NetCDF format and finally to .RAW files to allow processing in the Xcaliber Qual Browser program. For all data, peaks with relative heights of less than 5% of the largest peak were discarded from the analyses. The intensities for all peaks in the spectra were then added, and the individual intensity for each peak was divided by this sum so that the intensity for each ion could be reported as a percent of the total ion packet. The center of mass (COM) energy was calculated for all measurements taken on the QTOF as each fragmentation resulted from the collision of one gas molecule with one analyte anion. Data obtained using the LCQ ion trap are reported using the arbitrary electronvolt values reported by the instrument for all CID experiments.

Vibrational Spectroscopy. Infrared multiple-photon dissociation spectroscopy (IRMPD) experiments on the Na^+ dianion complex were performed using the Fourier-transform ion-cyclotron resonance mass spectrometer (FTICR-MS) beamline station[59] at the FELIX (free-electron laser for infrared experiments) facility[60] at the FOM Institute for Plasma Physics Rijnhuizen. The ions generated from 1 mM solution in each diastereomer of tartrate and NaOH by electrospray at −2 kV were held in a hexapole accumulation trap for 5 s before injection into the Penning trap of the FTICR-MS and irradiated for 3.5 s at a macropulse repetition rate of 10 Hz (energies up to 50 mJ/pulse), with 5 mass spectra averaged per spectral data point. The IRMPD yield spectrum is produced by dividing the sum of the fragment ion(s) by the sum of parent and fragment ion(s) as a function of FEL wavelength.

dx.doi.org/10.1021/jp3007156 | J. Phys. Chem. A 2012, 116, 4789−4800

3. RESULTS AND DISCUSSION

At first, we carried out an extensive theoretical search of the conformational space for every possible tartrate dianion isomer of both diastereomers (**T1**-**T4**, shown representatively for **Rac-2A** in Figure 3), and all isomers for each corresponding lower

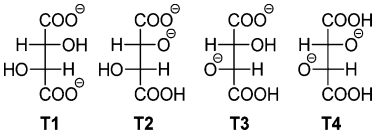

Figure 3. Tartrate dianion isomers of **Rac-2A** (shown as the L-isomer).

charge state, i.e., the radical anion and neutral diradical, of both diastereomers of tartaric acid were then studied. (Note: The L-form was used to calculate properties of the racemic compound.) It turned out that for the dianionic and radical anionic forms, isomer **T1** was the most stable, whereas the neutral diradical form prefers isomer **T4**. The most stable conformers for these isomers of the dianionic, radical anionic and diradical neutral form of the L- and meso forms together with important bonding parameters are shown in Figures 4a–c and 5a–c. For both dianions, we clearly see strong hydrogen bonding with rather short bond lengths to the carboxylate group, i.e., 1.797 Å for **Rac-2A** and 1.735/1.804 Å for **Meso-2A**. In both cases the $(C-O)_{carbox}-H-O$ torsion angle is close to 0°, i.e., 6.1° for **Rac-2A** and 2.6°/9.1° for the **Meso-2A**. The strength of this H-bond can be estimated from the energy required to rotate out one of the hydroxyl groups to a $(C-O)_{carbox}-H-O$ torsion angle of 90°/180°, which costs 16.4/11.6 kcal/mol for **Rac-2A** and 14.9/17.0 kcal/mol for **Meso-2A**. This is a substantial amount of energy, and clearly indicates very strong hydrogen bonding active in stabilizing the negative charges at the carboxylate groups.

In contrast, only one of the carboxylate groups in the monoanionic radicals shows a hydrogen bond, but with shorter bond lengths to the carboxylate group of 1.699 Å for **Rac-AR** and 1.828 Å for **Meso-AR**. Here the $(C-O)_{carbox}-H-O$ torsion angles are also close to 0°, i.e., 2.4° for **Rac-AR** and 4.9° for **Meso-AR**, and to rotate out the hydroxyl group responsible for the hydrogen bonding to a $(C-O)_{carbox}-H-O$ torsion angle of 90°/180° costs 20.0/23.8 kcal/mol for **Rac-AR** and 14.1/15.4 kcal/mol **Meso-AR**. For **Meso-AR**, there is an additional hydrogen bond of length 1.673 Å originating at the OH group. Modifying the torsional angle to 90°/180° costs 19.9/21.9 kcal/mol, respectively, here. Spin density plots (Figure 6a,c) for **Rac-AR** and **Meso-AR** show that the unpaired electrons can mainly be found at the carboxyl group not involved in hydrogen bonding. As for the neutral diradical, there is no hydrogen bonding anymore. In fact, for both diastereomers the most stable structure is one in which both unpaired electrons are situated at the two oxygen atoms bonded to C2 and C3. This is clearly seen in a plot of the spin densities shown in Figure 6b,d.

Dianionic forms of tartaric acid that do not place both of the charge on the carboxylates (Figure 3) were found to be of higher energy in this investigation for **Rac-2A** and **Meso-2A**, and these isomers will not be discussed in full detail. However, we note that shifting a hydrogen atom from the hydroxyl to the carboxylate group (**T1** → **T2**/**T3**) costs the dianion at least 20 kcal/mol, whereas for the neutral radical compounds the placement of the unpaired electron on the hydroxyl rather than

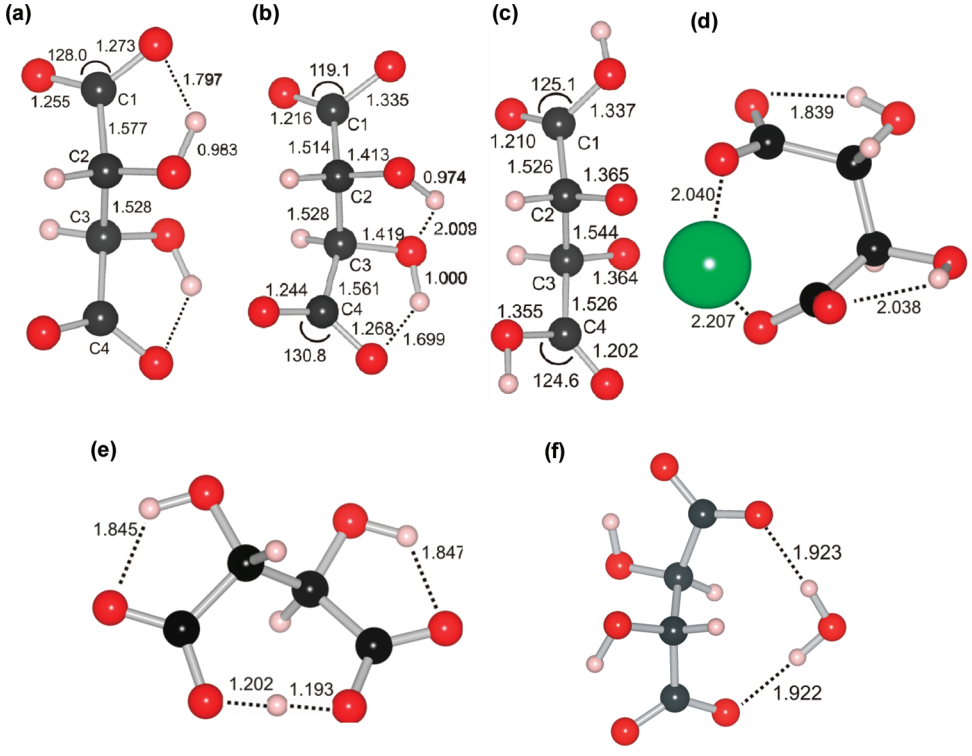

Figure 4. MP2/aug-cc-pVTZ structures for the most stable conformers of the (a) dianionic (**Rac-2A**), (b) radical anionic (**Rac-AR**), and (c) diradical neutral (**Rac-2R**) forms of L-tartaric acid as well as optimized structures of the lowest energy conformer of (d) the sodium complex (**Rac-2A-Na**$^+$), (e) the protonated monoanion (**Rac-A**), and (f) the H_2O adduct. The energies for structures (a), (b), (c), and (f) are shown in Table 1 given relative to the bare dianion.

dx.doi.org/10.1021/jp3007156 | J. Phys. Chem. A 2012, 116, 4789–4800

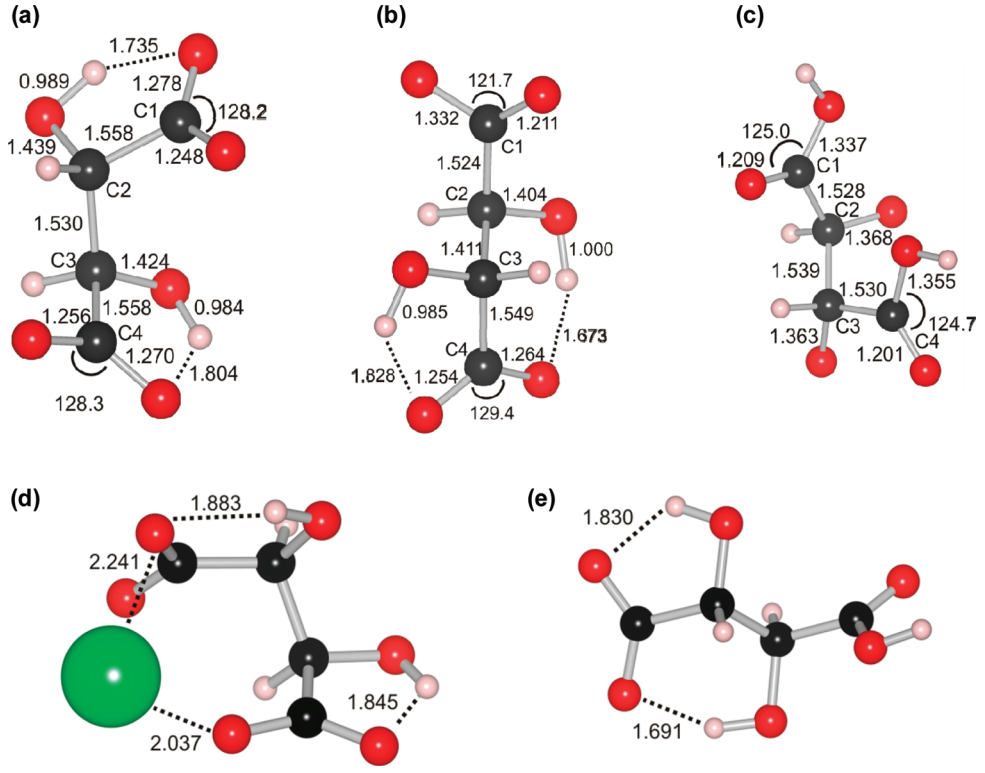

Figure 5. MP2/aug-cc-pVTZ structures for the most stable conformers of the (a) dianionic (**Meso-2A**), (b) radical anionic (**Meso-AR**), and (c) diradical neutral (**Meso-2R**) forms of *meso*-tartaric acid as well as optimized structures of the lowest energy conformer of (d) the sodium complex (**Meso-2A-Na**$^+$) and (e) the protonated monoanion (**Meso-A**). The energies for structures (a), (b), (c), and (f) are shown in Table 1 given relative to the bare dianion.

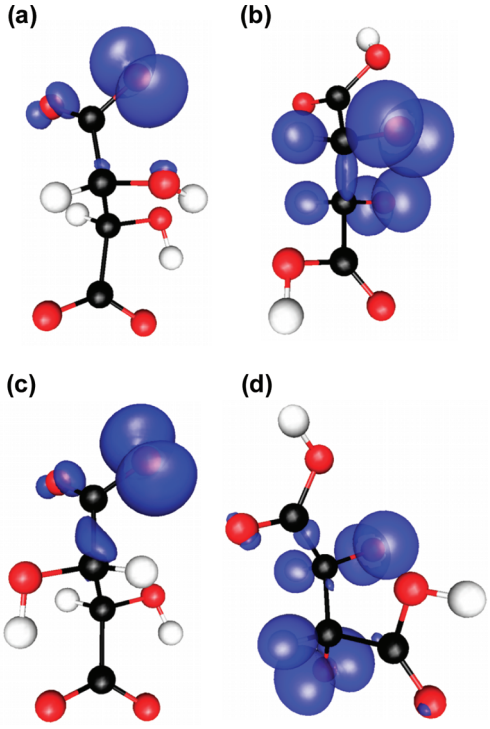

Figure 6. Spin densities (shown in blue) for the radical anionic (**Rac-AR**) and diradical neutral (**Rac-2R**) forms of L-tartaric acid: (a) **Rac-AR**, (b) **Rac-2R**, (c) **Meso-AR**, and (d) **Meso-2R**.

the carboxyl-oxygen atom only costs a few kcal/mol in energy. Of the four possible dianionic structures, the ones placing the charges on the C1 carboxylate and the C3 oxygen atom (**T3**) were close, although higher in energy than those displaying dicarboxylate anions (**T1**). The other possible isomers, (**T2** and **T4**) either dissociate or converge to an associated stable structure, e.g., **T1** or **T3**.

Concerning the stability of the dianion, the energy values in Table 1 clearly show that compared to the radical anionic forms the dianions **Rac-2A** and **Meso-2A** are very stable (by more than 20−30 kcal/mol) with respect to electron loss. The L-form **Rac-2A** is thus ∼5 kcal/mol more stable than **Meso-2A**, and thus our following analysis will begin with the more stable form, **Rac-2A**. It is well-known that to obtain accurate electron affinities one requires rather large basis sets, including diffuse and high angular momentum functions together with a sophisticated electron correlation procedure.[61−63] It is, however, computationally too demanding to carry out coupled-cluster calculations for such a large system going beyond double-ζ basis sets. We therefore adopted two different strategies, which lead to results quite close to each other.

It is well-known that second-order Møller−Plesset theory often overestimates electron correlation effects and has convergence difficulties with increasing order of the Møller−Plesset series expansion,[64−66] and this effect was seen in our previous study on aliphatic and aromatic dianions.[21] A comparison between the MP2 and CCSD(T) results with the aug-cc-pVDZ basis set shows that this is not the case here, as coupled cluster gives electron detachment energies for the dianions of 5−10 kcal/mol higher than the corresponding MP2 result. Nevertheless, at the MP2 level of theory we can estimate the CBS limit, which gives an adiabatic electron detachment energy for **Rac-2A** of 26.2 kcal/mol. Adding the difference MP2(CBS) − MP2(aug-cc-pVDZ) to the CCSD(T)/aug-cc-pVDZ result, we can now estimate the CBS limit at the CCSD(T) level of

dx.doi.org/10.1021/jp3007156 | J. Phys. Chem. A 2012, 116, 4789−4800

Table 1. Relative Energies (kcal mol^{-1}) for Best Conformers of the Tartaric Acid Dianion and the Products of Electron Detachment from the Dianion

	MP2/aug-cc-pVDZ[a]	MP2/aug-cc-pVTZ[d]	MP2/aug-cc-pVQZ[a]	MP2/CBS[a]	CCSD(T)/ aug-cc-pVDZ[a]	CCSD(T)/ aug-cc-pVDZ[a] +ΔMP2[c]	CCSD(T)-F12/VDZ-F12[a]
Rac-2A	0.0	0.0 (0.0)	0.0	0.0	0.0	0.0	0.0
Rac-AR[b]	23.5	26.8	28.5	29.8			
Rac-AR	20.8	23.6 (23.5)	25.1	26.2	32.4	37.8	35.4
Rac-2R	126.0	132.2 (131.3)	135.1	137.3	110.4	121.6	119.6
Meso-2A	4.8	4.7 (4.5)	4.7	4.7	4.7	4.7	4.7
Meso-AR[b]	34.4	36.6	39.0	40.8			
Meso-AR	17.5	20.1 (19.6)	21.6	22.7	25.6	30.8	28.4
Meso-2R	126.3	132.5 (131.3)	135.4	137.6	110.4	121.7	129.5

[a]Calculated as single points on MP2/aug-cc-pVTZ geometries. [b]Calculated at geometries of the optimized dianion to obtain the VEDE's. [c]CCSD(T)/ aug-cc-pVDZ results corrected to the MP2 CBS limit based on TZ/QZ-extrapolation as in ref 45 eq 1. [d]Values in parentheses include zero-point vibrational corrections.

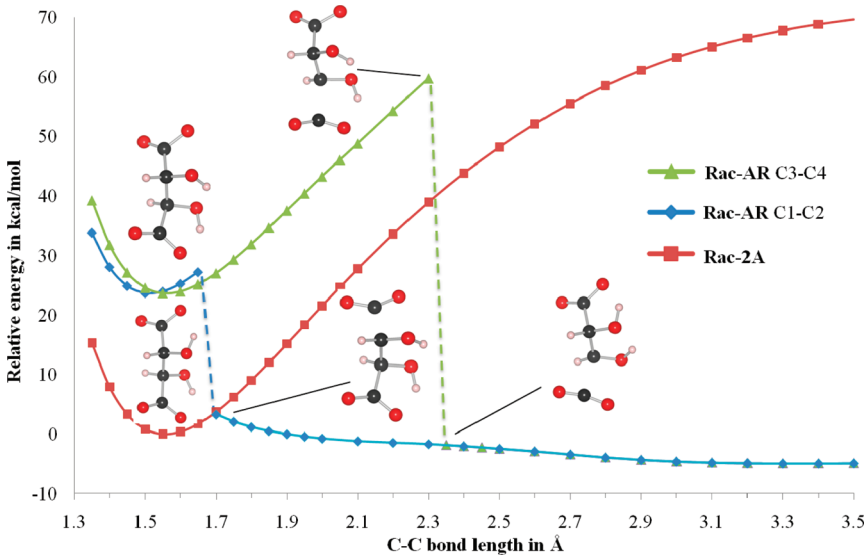

Figure 7. Decomposition path into $(O_2C{-}CH(OH){-}CH(OH))^-$ and CO_2 at the MP2/aug-cc-pVTZ level of theory shown as a scan of bond-breaking C−C bond lengths for the isomers **Rac-AR** and **Rac-2A**.

theory, which gives 37.8 kcal/mol. This is in excellent agreement with the CCSD(T)-F12/cc-pVDZ-F12 value of 35.4 kcal/mol. Hence both methods, CCSD(T)-F12 and CCSD(T)+ΔMP2, give similar results, not only for the first but also for the second detachment energy; the latter is estimated to be around 120 kcal/mol. This confirms results from a very recent study where CCSD(T)-F12 was found to perform well for interstellar anions.[67] The results clearly show the very high thermodynamic stability of the dianions **Rac-2A** and **Meso-2A** (with respect to electron loss), which is due to strong hydrogen bonding. Thus hydrogen bonding greatly enhances the stability of dianions by reducing the Coulomb repulsion between (de)localized charges. To discuss the overall stability of this dianion, we need to think about not only electron detachment but also decomposition via C−C bond dissociation with loss of CO_2 combined with the loss of an electron, i.e.,

$$(O_2C{-}CH(OH){-}CH(OH){-}CO_2)^{2-} \rightarrow (O_2C{-}CH(OH){-}CH(OH))^{\bullet -} + CO_2 + e^-$$

We briefly note that CO_2^- is only metastable at a bent geometry at 0.6 eV above CO_2 and autoionizes while becoming linear (see the work of Gutsev, Bartlett, and Compton[68] or Schwarz and co-workers[69]); hence we do not consider CO_2^- here. The calculated reaction path for **Rac-2A** is shown in Figure 7, which clearly shows that the dianion is thermodynamically unstable with respect to decomposition; i.e., it can autoionize upon release of CO_2. The potential hypersurface is rather complicated and involves rotation of the hydroxyl group shown in the graph by the steep descent of the radical anion path (**Rac-AR**), crossing with the dianion path at C1−C2 distance of about 1.70 Å. The rather steep descent suggests that for a more complete picture of the decomposition hypersurface a multireference treatment is required. Nevertheless, for the radical anion **Rac-AR**, we find a transition state toward dissociation with a C1−C2 distance of 1.632 Å and an imaginary frequency of 1170i cm^{-1}. This transition state is only 4.0 kcal/mol higher in energy than **Rac-AR.** The curve crossing with the dianion occurs at an energy of 3.3 kcal/mol relative to **Rac-2A.** The resulting dissociated (anionic) structure is 4.9 kcal/mol more stable than **Rac-2A.** Finite temperature effects (entropy) will even further enhance the decomposition and subsequent release of CO_2. Thus, although the dianion is thermodynamically stable with respect to direct electron detachment, it is only metastable with respect to dissociation. Moreover, Table 2 shows that entropy effects clearly favor the dissociation, and

dx.doi.org/10.1021/jp3007156 | J. Phys. Chem. A 2012, 116, 4789−4800

Table 2. Reaction Energies, Enthalpies, Entropies, and Free Energies (at Standard Temperature and Pressure) of CO_2 Dissociation vs Other Dissociation Channels for Lowest Energy Conformers of the Tartrate Dianion and Dianion Complexes Investigated at the MP2 level of theory (All in kcal mol^{-1})[a]

	MP2								
reaction	ΔE	ΔH	ΔG	$T\Delta S$	B3LYP[b] ΔE	PBE[b] ΔE	PW91[b] ΔE	LDA[b] ΔE	CCSD(T)/ aug-cc-pVDZ ΔE
Rac-2A									
Rac-2A → $[C_3O_4H_4]^-$ + CO_2 + e^-	1.1	−2.2	−10.2	8.1	−25.3	−25.4	−23.5	−7.1	0.5
Rac-2A-H2O-1									
Rac-2A-H2O-1 → $[C_3O_4H_4(H_2O)]^-$ + CO_2 + e^-	10.2	7.5	−2.9	10.4	1.7	1.6	3.6	20.8	9.7
Rac-2A-H2O-1 → **Rac-2A** + H_2O	23.5	21.3	10.6	10.6	39.4	40.5	41.0	47.1	23.9
Rac-2A-Na$^+$									
Rac-2A-Na$^+$ → $[C_3O_4H_4(Na)]$ + CO_2 + e^-	91.2	89.0	78.9	10.1	77.8	77.8	79.8	98.2	83.0
Rac-2A-Na$^+$ → **Rac-2A** + Na^+	226.9	225.8	216.8	8.9	234.0	231.9	232.7	238.6	206.2
Rac-2A-Na$^+$ → $Na[CH(OH)CO_2]$ + $[CH(OH)CO_2]^-$	97.6	92.5	78.2	14.3	106.6	103.2	103.9	121.9	120.2

[a]Energies from density functional and CCSD(T) calculations are given as well. The aug-cc-pVTZ basis set was employed unless otherwise noted. [b]Employing MP2/aug-cc-pVTZ geometries.

very low temperatures are needed to trap this dianion. This result is in agreement with the failure to observe the bare tartrate dianion under standard ionization conditions unless extreme care is taken and implies that the dianion needs to be investigated experimentally under exceedingly gentle conditions. Previous experimental studies of aromatic dicarboxylate dianions[70] demonstrated the metastability with respect to decarboxylation and electron loss, and it is clear that this effect is exacerbated in the current system. This is presumably due to the lack of aromatic stabilization, and although the internal hydrogen bonding in the dianion is quite strong, it is not sufficient to prevent this facile process. Similarly, it is observed that CID of the dianion shows no smaller m/z dianion fragments, suggesting that all the fragments are too small to sustain the double charge, similar to the case with the aromatic dicarboxylate dianions.

The favored thermodynamic decomposition of the bare tartrate dianion into CO_2 + e^- makes it very difficult to observe this species experimentally, for example, by mass spectrometry. Experimental studies of this dianion using electrospray ionization to introduce the species into either a quadrupole-time-of-flight (QTOF) or ion trap mass spectrometer (LCQ) under standard conditions did not lead to any observable dianion. Instead, the fragments of this molecule arising from McLafferty rearrangement (Scheme 1) were observed. This

Scheme 1

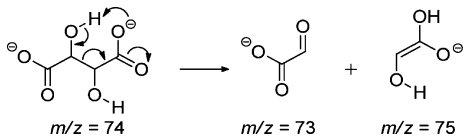

rearrangement gave two fragments in this case, both with the mass to charge (m/z) of 75, which could be differentiated from the parent m/z of 74 for the tartrate dianion due to the mass resolution of the instruments. After these observations, focus was placed on using the LTQ ion trap mass spectrometer in an attempt to measure the dianion. It was reasoned that the ability to collect, i.e., trap, ions for long periods in this instrument might allow a sufficient number of tartrate dianions to be collected for study. When the ion collection time for this MS was increased from the typical 50 ms to 8 s, and the ionization temperature was decreased to the minimum needed for introduction of the molecule into the gas phase, a signal corresponding to the tartrate dianion could be observed. Using these trapping parameters, both the racemic dianion (**Rac-2A**) and the rearranged fragment could be detected separately depending on the capillary temperature. It was thus found that 160 °C was the optimum temperature to detect the tartrate dianion. Though modifications of the standard parameters on the LTQ ion trap allowed us to observe the dianion, the He used as the collision gas in the ion trap was not optimal for determining the center-of-mass collision energy necessary for dissociation. Despite this complication, a study of the stability of the tartrate dianion was still performed using the LTQ ion trap MS because detecting of the dianion was extremely difficult using other instruments.

CID experiments were then performed with this instrument by increasing the collision energy stepwise by 1 arbitrary energy unit increments (note that these arbitrary energy units are roughly calibrated to equal 1 eV). The limitation of this experiment using an ion trap MS was that He induced dissociation requires multiple collisions with the ions that are held in the trap; therefore, the energy from only a single collision cannot be calculated. As previously mentioned, the stability of the tartaric acid dianion is low; however, some data concerning the stability of **Rac-2A** were obtained with some difficulty. The data from the CID experiments of the parent dianion are presented in Figure 8a. The labile nature of the tartrate dianion manifested itself in the trapped ion packets as well, and the dianion tended to form an adduct from water present in the trap to stabilize the double negative charge. This was the case even though mass selection of the parent ion for **Rac-2A** was performed. Presumably, the adduct was still visible due to water coming from fragmentation of the dianion during or slightly after trapping. (Figure 8b). This created difficulties in the measurement and characterization of the fragmentation reactions in this experiment as the hydrate of **Rac-2A** was seen randomly at different energies on different replicates (data not shown). If observed, the adduct could not be removed from the tartrate ion, even if an increased collision energy was used to attempt to disrupt the association of these molecules. However, a sufficient concentration of the naked dianion was trapped to allow fragmentation data of this species to be collected, and these data indicate that the threshold of dissociation is low. The measured value was ∼13−14 arbitrary collision units, which are roughly equal to an eV/unit, for the tartrate dianion. If this

dx.doi.org/10.1021/jp3007156 | J. Phys. Chem. A 2012, 116, 4789−4800

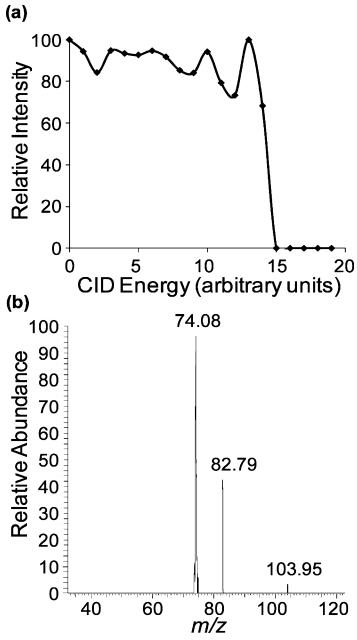

Figure 8. Collisionally induced dissociation of **Rac-2A**. (a) Threshold of dissociation from the CID experiments performed on the tartaric acid dianion. (b) Mass spectrum of the tartaric acid dianion with a collision energy of 3 eV. The m/z of 74 is the parent dianion, m/z of 83 is proposed to be the parent dianion complexed to water and the m/z of 104 is proposed to be the radical anion of **Rac-2A** formed from the loss of an electron and CO_2 (Scheme 2).

value is converted to a center-of-mass energy assuming a single collision with He, the threshold would be estimated to be ~0.35 eV; however, this conversion is not entirely accurate due to the multiple collisions. These results indicate that this isomer is very unstable and will associate with adducts for stability, if possible. One other fragment observed during these experiments was of interest as it corroborated the theoretical calculations, which showed that expulsion of CO_2 and an electron from the dianion should be an accessible decomposition pathway (Figure 7). Specifically, a fragment with a m/z of 104 was regularly observed during fragmentation of the dianion (Figure 8b). This mass is consistent with the radical anion that should be the product after loss of CO_2 and an electron (Scheme 2), and these data show that the calculated

Scheme 2

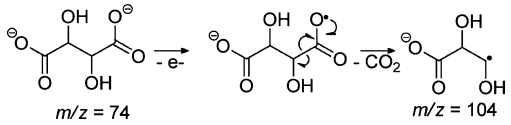

decomposition path of the unstable dianions of dicarboxylic acids is operative. Further, the repulsive Coulomb barrier toward dissociation does not appear to enhance the stability of the dianion to the degree that would be theoretically expected from dissociating point charges. This effect was previously observed in the combined decarboxylation/detachment process of aromatic carboxylate dianions[70] and is presumably due to delocalization of the negative charge into the extended π system during the $CO_2 + e^-$ loss process.

The observation of the water adduct in the mass spectrum is indicative of the relative instability of the dianion in contrast to the relative stability of its water or H^+ and Na^+ cation complexes. To highlight the similarity of stabilization between Na^+ complexation and addition of a H^+ to form the monoanion, we refer to the latter as the H^+ adduct. It should be noted that this additional H^+ could stabilize both carboxylate sites via intramolecular proton transfer (Scheme 3), effectively reducing

Scheme 3

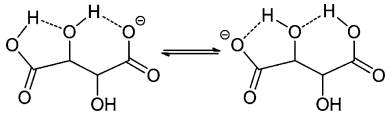

the gas-phase acidity of the singly deprotonated monoanion. Concerning the uptake of H_2O by the tartrate dianion the MP2/aug-cc-pVTZ level of theory gives conformer **Rac-2A-H_2O-1** with two hydrogen bridges from the water molecule to the oxygen atoms of both carboxyl groups as the most stable structure, as seen in Figure 4f. The dissociation energy for this complex is 23.5 kcal mol^{-1} at the MP2/aug-cc-pVTZ level of theory, which points to very strong hydrogen bonds. This is supported by the rather short bond distance of around 1.92 Å. The next most stable structure involves bridging both oxygen atoms at one CO_2 unit (conformer **Rac-2A-H_2O-2**), which is only 0.6 kcal mol^{-1} less favorable. The structure that results from the bridging of one CO_2 and one OH group (conformer **Rac-2A-H_2O-3**) is 1.2 kcal mol^{-1} less stable than **Rac-2A-H_2O-1**, although the hydrogen bonds are shorter (see Figure S1 in the Supporting Information). No other energetically low-lying conformer could be found, especially none bridging the two OH groups. The conclusions from our gas-phase investigations of H_2O complexes of tartaric acid can also help to shed light on the behavior of solvated tartaric acid. A recent contribution combining electronic circular dichroism with quantum chemical calculations at the B3LYP/6-31+G(d) level focused on **Rac-2A** and the H_2O adduct.[71] Although a different optimal structure was found in that study (H_2O added to one carboxylate group), the computational level used in our study (MP2/aug-cc-pVTZ) indicates the structure bridging both carboxyl groups as being the lowest in energy by a small margin (0.5 kcal mol^{-1}). The high affinity for water explains the experimental observation of the water adduct formed during the CID experiments of the dianion.

The tartrate dianion was also computed to have a high affinity for Na^+ complexation. As per the procedure described previously, a minimum structure of the Na^+ dianion complex was found and is named **Rac-2A-Na^+**, which places the Na^+ ion between the carboxylate groups (Figures 4d). This complex has a Na^+ affinity of 226.9 kcal mol^{-1} (9.8 eV) calculated at the MP2/aug-cc-pVTZ level of theory for dissociation of Na^+. As a comparison, Na^+ bonding strength with that of a representative covalent bond in the complex, the strength of the C−C bond in **Rac-2A-Na^+** is estimated to be 97.6 kcal mol^{-1} through thermodynamic calculation of the fragmentation reaction (**Rac-2A-Na^+** → $^-O_2C-CH(OH)$ + Na^+ $^-O_2C-CH(OH)$). Thus the Na^+ binding energy is very high compared to the C−C bond energy, and it is expected that fragmentation of the hydrocarbon will occur before loss of the Na^+. The meso-diastereomer **Meso-2A-Na^+** (Figure 5d) is less stable than **Rac-2A-Na^+** by 2.9 kcal/mol. As for the latter, it takes a large amount of energy (234.5 kcal mol^{-1}) to remove the sodium cation.

With the theoretical data concerning the stability of the sodium-coordinated dianion in hand, attention was focused on

dx.doi.org/10.1021/jp3007156 | J. Phys. Chem. A 2012, 116, 4789−4800

the experimental investigation of this species via MS. A peak with m/z of 171 that corresponds to the sodium adduct of the tartrate dianions could be easily observed by ESI-MS on either the LTQ ion trap or QTOF. This alone indicated that this species was more stable than the naked tartrate dianion and allowed experiments to be performed on the QTOF, which was capable of using N_2 to activate CID of the molecule from a single collision. To maximize the signal from the sodium adduct (**Rac-2A-Na**$^+$ and **Meso-2A-Na**$^+$), 1 mol equiv of NaOH was added to the tartaric acid solution. Although the initial focus was placed on studying chiral racemic tartaric acid, the higher stability of the sodium adduct facilitated experimentation to the point that this study was expanded to include the sodium adduct of the meso tartrate dianion as well. This allowed an interesting question to be addressed both computationally and experimentally. Specifically, if and how does the spatial arrangement of the atoms in a tartaric acid sodium complex affect the ability of the molecule to stabilize two negative charges? The difference in the dissociation threshold for these diastereomers was calculated to be 2.9 kcal/mol at the MP2/aug-cc-pVTZ level of theory, and it was found that the sodium adduct of the racemic compound was thermodynamically more stable. However, the sodium adduct of the racemic compound was also found to begin fragmenting with collisions at a center of mass energy (COM) of ~22.62 kcal/mol, which was 6.49 kcal/mol lower in energy than collisions necessary to dissociate the sodium adduct of the meso compound (Figure 9). These data

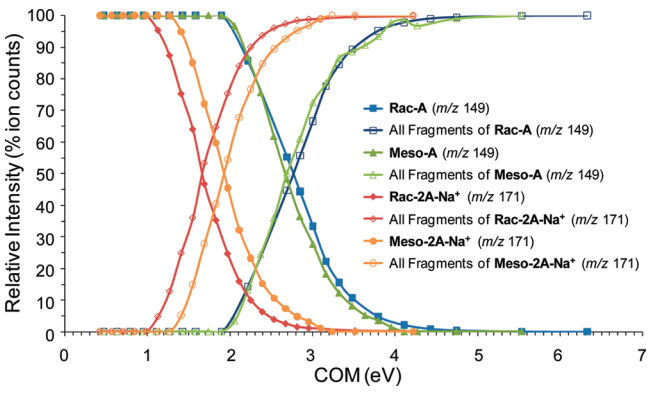

Figure 9. Collisionally induced dissociation thresholds of **Rac-2A-Na**$^+$ and **Meso-2A-Na**$^+$ (m/z 171) as well as **Rac-A** and **Meso-A** (m/z 149).

suggest that fragmentation is a kinetic process, in which the dissociation of the thermodynamically more stable sodium adduct of the racemic tartrate dianion proceeds via a lower energy transition state than that of the corresponding meso compound. The fragmentation pattern of these two molecules was nearly identical, however, indicating that sodium cation does not differentially stabilize any of the constituent bonds between the diastereomers (see Figure S2 in the Supporting Information).

The calculated structures and stabilities of the Na^+ dianion complexes were investigated spectroscopically by IRMPD, revealing a strong influence of the Na^+ cation on the vibrations of the dianion. Irradiation of the singly charged **Rac-2A-Na**$^+$ and **Meso-2A-Na**$^+$ complexes with an infrared laser produced a photofragmentation pattern similar to that observed from CID, and as computationally predicted, the dissociation was not via loss of the metal cation, but rather dissociation of covalent bonds, demonstrating the strength of the complexation interaction. Shown in Figure 10a,b are the experimental infrared action spectra obtained by on-resonance dissociation (IRMPD) of the complexes. As would be expected, the IRMPD spectra of the diastereomer complexes are quite similar, but there are subtle differences that are revealed by inspection. For the **Meso-2A-Na**$^+$ complex relative to the **Rac-2A-Na**$^+$ complex, the longest-wavelength spectral feature at ~1050 cm^{-1} is blue-shifted and the double-peak feature at ~1600 cm^{-1} shows a greater splitting. Both spectra show the dominant IR-absorption features expected from a hydrocarbon with primary alcohol and carboxylate functional groups. Namely, the band at ~1050 cm^{-1} is due primarily to the C−O stretch of the alcohol groups, the intensity of the feature at ~1350 cm^{-1} is largely due to the carboxylate symmetric stretch modes and the ~1600 cm^{-1} bands are from the antisymmetric stretching modes of the carboxylate (Figure 10). To aid in the spectral interpretation and help validate the computational results, the spectra were compared to both harmonic (scaled by a factor of 0.965) and anharmonic (unscaled) calculated vibrational frequencies (Tables S2 and S6 in the Supporting Information). Although the agreement between experimental and calculated values for anharmonic frequencies is usually very good, it was found that the scaled harmonic frequencies more correctly predicted the experimentally observed spectra in this study (Supporting Information Figure S3). Shown overlaid in the upper two panels of Figure 10 are the computed scaled harmonic vibrational frequencies of **Meso-2A-Na**$^+$ and **Rac-2A-Na**$^+$ convoluted with a 20 cm^{-1} full-width half-maximum Gaussian line shape to provide simulated spectra. Overall, the experimental spectra correlate well with the theoretical predictions, giving confidence in the proposed structure and relative energy of the **Rac-2A-Na**$^+$ and **Meso-2A-Na**$^+$ complexes.

To aid the spectral interpretation of the influence of the Na^+ cation on the dianion, the computed infrared spectrum (at the same level of theory) of the uncomplexed dianion is shown in Figure 10c. Comparison of the predicted vibrational spectrum from the bare dianion to the observed and predicted vibrational spectrum from the Na^+ complexes shows a large splitting of the antisymmetric carboxylate stretches (located at ~1640 cm^{-1} according to the anharmonic frequency calculations) induced by the Na^+ binding, demonstrating a strong influence on the dianion. The frequency of this vibrational mode in a bare carboxylate such as benzoate is at ~1626 cm^{-1},[72] which is very similar to the 1636 and 1638 cm^{-1} anharmonic values (Table S6) predicted here for the tartrate dianion. The frequencies for these vibrational modes in the dianion are similar for both carboxylate groups because of the nearly identical chemical environments of both carboxylates, as shown by Figure 4a. However, as shown by the structure in Figure 4d, the complexation of a Na^+ ion to the dianion results in very different chemical environments for the two carboxylate groups. This effect produces a red shift of one antisymmetric stretch frequency and a blue shift of the other, resulting in the splitting of these bands observed in the IRMPD spectrum and computations that is shown in Figure 10. For comparison, the IR spectrum of the solid-state sodium benzoate complex shows a vibrational frequency of 1553 cm^{-1},[73] a red shift that is qualitatively similar to the red shift observed and computed for the antisymmetric stretch mode of the carboxylate group of the tartrate dianion that is most closely complexed to the Na^+ ion. This band is generally a sensitive spectroscopic indicator of the complexation interactions, and the significant splitting of the feature indicates a strong binding interaction between the dianion and the cation.

dx.doi.org/10.1021/jp3007156 | J. Phys. Chem. A 2012, 116, 4789−4800

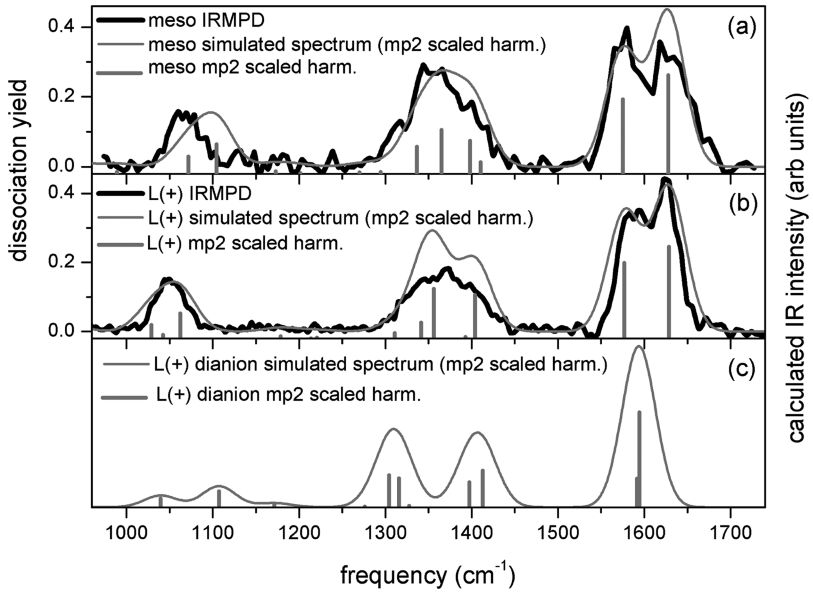

Figure 10. IRMPD spectrum (a) of **Meso-2A-Na**$^+$ dianion complex (black) compared to simulated spectrum (gray) (b) of **Rac-2A-Na**$^+$ (black) and simulated spectrum (gray) and (c) **Rac-2A** dianion spectrum (gray) calculated from structure **Rac-2A** at MP2/aug-cc-pVTZ level of theory. Simulated spectra are from scaled (0.965) harmonic frequencies. Intense spectral features are primarily due to symmetric and antisymmetric carboxylate stretching modes and the C−O stretch of alcohol.

In addition to the general features that clearly demonstrate the strong influence of the complexed Na^+ cation on the dianion internal bonding, there are more subtle but clear distinctions between the spectra of the diastereomers that point to a difference in the Na^+ complexation interaction. The most likely explanation for the ∼1050 cm^{-1} band shift is that the primary alcohol C−O stretch vibrational modes are being influenced by intramolecular hydrogen-bonding differently for two diastereomers. The optimized structures shown for **Meso-2A-Na**$^+$ and **Rac-2A-Na**$^+$ show a slightly less overall distance for the hydroxyl group hydrogen-bonding to the carboxylate group, suggesting a stronger interaction. A blue shift of the band at ∼1050 cm^{-1} is commensurate with an increase in the C−O bonding strength, which would be expected from the decrease in the OH-bonding strength due to increased hydrogen donor bonding with the carboxylate groups. This interaction would also be expected to increase the perturbation on the antisymmetric stretches responsible for the splitting of the dianion bands seen at ∼1600 cm^{-1}. The strength of the carboxylate−Na^+ interaction is such that it might be expected that this interaction with the OH group would be largely hidden, yet as seen in the experimental data of Figure 10a,b, the splitting of the meso complex is slightly enhanced relative to the chiral complex, in agreement with the interpretation of increased perturbation by the hydroxyl group. Though the scaled harmonic frequency calculations do not recover the clear experimental differences between the diastereomers regarding the splitting of this band, the anharmonic frequency calculations (as shown in Figure S3, Supporting Information) do. Thus, it is quite interesting that the complexation behavior of the diastereomers is sufficiently different that the spectroscopy shows interpretable shifts, and the success of the vibrational frequency calculations to model the IRMPD data lends confidence toward the computed structures and energetics of the tartarate dianion and complexes. Additional tables listing the computed frequencies are given in the Supporting Information (Tables S1−S6 in the Supporting Information).

As a final test of the ability of adducts to stabilize the racemic and meso tartrate, the extreme case of a proton adduct or monoanion was studied both theoretically and experimentally. From calculations at the MP2/aug-cc-pVTZ level of theory, the racemic monoanion **Rac-A** was again found to be more stable than the corresponding meso compound **Meso-A** by 10.1 kcal/mol. The protonated form **Rac-A** is thereby more stable than **Rac-2A** by 425.1 kcal mol^{-1} (MP2/aug-cc-pVTZ), underlining the low stability of the dianionic form. The threshold for dissociation of each species was then measured via ESI-MS with the QTOF MS using N_2 as the collision gas. In this case, both monoanions began to fragment at the same COM collision energy, indicating that the barrier to dissociation was equal between them (Figure 9). The minimum energy necessary to begin dissociation of either the racemic or meso monoanion was ∼47.2 kcal/mol, indicating that the H^+ adduct was better able to stabilize the two negative charges than the Na^+ adduct. For the monoanions, the fragmentation pattern of the racemic and *meso* compounds varied (Figure S4 in the Supporting Information), presumably from differential intramolecular hydrogen bonding ability in the molecules due to the different spatial arrangement of the atoms, which was also observed in our calculations.

4. CONCLUSION

We presented the first comprehensive study of the thermodynamic and kinetic stability of the tartaric acid dianion. The gas-phase stability of the doubly deprotonated tartaric acid dianion is experimentally and computationally demonstrated to be significantly enhanced by intramolecular hydrogen bonding or by complexation with cations such as Na^+. Experimentally we were able to measure the dissociation threshold for the bare tartaric acid dianion, the sodium adduct and the proton adduct. These data show the bare dianion is the least stable of these molecules and adding stabilization factors such as a water molecule, sodium ion or a proton decreases the ease of dissociation. The water adduct is unable to be isolated in the mass spectrum and

dx.doi.org/10.1021/jp3007156 | J. Phys. Chem. A 2012, 116, 4789−4800

the resulting experimental inference that the water is the least stabilizing is corroborated by computations. The energy-resolved, collision-induced dissociation of the sodium and proton adducts are measured and the proton stabilizes the dianion toward dissociation more so than sodium, in line with the fact that the H^+ addition energy is higher than the Na^+ complexation energy. The fragmentation for the meso and racemic forms of the proton adducts are nearly identical whereas the difference in dissociation for the sodium adduct suggests a greater stability of the sodium complex with the meso form of the tartrate dianion. The photodissociation-based infrared spectroscopy of Na^+ complexes reveals a strong perturbation on the bonding of the dianion by the complexation of a sodium ion, and spectroscopic differences between the diastereomers are consistent with the trend in the calculated stabilization energies.

■ ASSOCIATED CONTENT

Supporting Information

Additional figures and tables from experimental and theoretical studies including structures, vibrational frequencies, and mass spectrometry data. This material is available free of charge via the Internet at http://pubs.acs.org.

■ AUTHOR INFORMATION

Corresponding Authors

*E-mail: S.R.C., campagna@ion.chem.utk.edu; R.N.C., compton@ion.chem.utk.edu.

Present Address

[∇]Sandia National Laboratories, Livermore, CA 94550, USA

Notes

The authors declare no competing financial interest.

■ ACKNOWLEDGMENTS

R.T. is grateful to the Alexander von Humboldt Foundation for financial support via a Feodor-Lynen fellowship, and P.S. for a Humboldt Research Award. P.S. is also grateful to Prof. G. Frenking (Marburg) for being such a wonderful host during the research stay in Marburg. We also acknowledge the support of Drs. Britta Redlich and Lex van der Meer as well as others of the FELIX staff. A.L.M. and R.N.C. were supported by the NSF (CHE-0848487).

■ REFERENCES

(1) Gawronski, J.; Gawronska, K. *Tartaric and Malic Acids in Synthesis*; Wiley: New York, 1999.
(2) Kliewer, W. M.; Howarth, L.; Omori, M. *Am. J. Enol. Vitic.* **1967**, *18*, 42.
(3) Stern, F.; Beevers, C. A. *Acta Crystallogr.* **1950**, *3*, 341.
(4) Maga, J. A.; Tu, A. T. *Food additive toxicology*; CRC Press: Boca Raton, FL, 1995.
(5) Gal, J. *Chirality* **2011**, *23*, 1.
(6) Polavarapu, P. L.; Ewig, C. S.; Chandramouly, T. *J. Am. Chem. Soc.* **1987**, *109*, 7382.
(7) Wu, L. M.; Clark, R. L.; Cooks, R. G. *Chem. Commun.* **2003**, 136.
(8) Rychlewska, U.; Warzajtis, B.; Hoffmann, M.; Rychlewski, J. *Molecules* **1997**, *2*, 106.
(9) Kohn, L. D.; Jakoby, W. B. *J. Biol. Chem.* **1968**, *243*, 2465.
(10) Castaldi, G.; Cavicchioli, S.; Giordano, C.; Uggeri, F. *J. Org. Chem.* **1987**, *52*, 3018.
(11) Dreuw, A.; Cederbaum, L. S. *Chem. Rev.* **2002**, *102*, 181.
(12) Sommerfeld, T. *Phys. Rev. Lett.* **2000**, *85*, 956.
(13) Hellemans, A. *Science* **1998**, *280*, 1009.
(14) Scheller, M. K.; Compton, R. N.; Cederbaum, L. S. *Science* **1995**, *270*, 1160.
(15) Sommerfeld, T.; Riss, U. V.; Meyer, H. D.; Cederbaum, L. S. *Phys. Rev. Lett.* **1997**, *79*, 1237.
(16) Bruna, P. J.; Mawhinney, R. M.; Grein, F. *J. Phys. B-At. Mol. Opt. Phys.* **1996**, *29*, 2413.
(17) Scheller, M. K.; Cederbaum, L. S. *J. Phys. B-At. Mol. Opt. Phys.* **1992**, *25*, 2257.
(18) Boldyrev, A. I.; Simons, J. *J. Chem. Phys.* **1993**, *98*, 4745.
(19) Boldyrev, A. I.; Simons, J. *J. Phys. Chem.* **1994**, *98*, 2298.
(20) Schwerdtfeger, P.; Hammerl, A.; Wesendrup, R. *Int. J. Mass Spectrom.* **2003**, *228*, 341.
(21) Tonner, R.; Lein, M.; Wesendrup, R.; Schwerdtfeger, P. *Theor. Chem. Acc.* **2010**, *126*, 129.
(22) Sommerfeld, T. *J. Am. Chem. Soc.* **2002**, *124*, 1119.
(23) Scheller, M. K.; Cederbaum, L. S. *J. Chem. Phys.* **1993**, *99*, 441.
(24) Weikert, H. G.; Cederbaum, L. S. *J. Chem. Phys.* **1993**, *99*, 8877.
(25) Weikert, H. G.; Cederbaum, L. S.; Tarantelli, F.; Boldyrev, A. I. *Z. Phys. D-At. Mol. Clusters* **1991**, *18*, 299.
(26) Middleton, R.; Klein, J. *Phys. Rev. A* **1999**, *60*, 3515.
(27) Tomita, S.; Andersen, J. U.; Cederquist, H.; Concina, B.; Echt, O.; Forster, J. S.; Hansen, K.; Huber, B. A.; Hvelplund, P.; Jensen, J.; Liu, B.; Manil, B.; Maunoury, L.; Nielsen, S. B.; Rangama, J.; Schmidt, H. T.; Zettergren, H. *J. Chem. Phys.* **2006**, 124.
(28) Limbach, P. A.; Schweikhard, L.; Cowen, K. A.; McDermott, M. T.; Marshall, A. G.; Coe, J. V. *J. Am. Chem. Soc.* **1991**, *113*, 6795.
(29) Wang, X. B.; Nicholas, J. B.; Wang, L. S. *J. Chem. Phys.* **2000**, *113*, 653.
(30) Skurski, P.; Simons, J.; Wang, X. B.; Wang, L. S. *J. Am. Chem. Soc.* **2000**, *122*, 4499.
(31) Herbert, J. M.; Ortiz, J. V. *J. Phys. Chem. A* **2000**, *104*, 11786.
(32) Maas, W. P. M; Nibbering, N. M. M. *Int. J. Mass Spectrom. Ion Processes* **1989**, *88*, 257.
(33) Enlow, M.; Ortiz, J. V. *J. Phys. Chem. A* **2002**, *106*, 5373.
(34) Wang, X. B.; Wang, L. S. *Nature* **1999**, *400*, 245.
(35) Wang, X. B.; Ding, C. F.; Wang, L. S. *Phys. Rev. Lett.* **1998**, *81*, 3351.
(36) Fleming, G. J.; Adib, K.; Rodriguez, J. A.; Barteau, M. A.; Idriss, H. *Surf. Sci.* **2007**, *601*, 5726.
(37) Frisch, M. J.; Trucks, G. W.; Schlegel, H. B.; Scuseria, G. E.; Robb, M. A.; Cheeseman, J. R.; Montgomery, J. A., Jr.; Vreven, T.; Kudin, K. N.; Burant, J. C.; Millam, J. M.; Iyengar, S. S.; Tomasi, J.; Barone, V.; Mennucci, B.; Cossi, M.; Scalmani, G.; Rega, N.; Petersson, G. A.; Nakatsuji, H.; Hada, M.; Ehara, M.; Toyota, K.; Fukuda, R.; Hasegawa, J.; Ishida, M.; Nakajima, T.; Honda, Y.; Kitao, O.; Nakai, H.; Klene, M.; Li, X.; Knox, J. E.; Hratchian, H. P.; Cross, J. B.; Bakken, V.; Adamo, C.; Jaramillo, J.; Gomperts, R.; Stratmann, R. E.; Yazyev, O.; Austin, A. J.; Cammi, R.; Pomelli, C.; Ochterski, J. W.; Ayala, P. Y.; Morokuma, K.; Voth, G. A.; Salvador, P.; Dannenberg, J. J.; Zakrzewski, V. G.; Dapprich, S.; Daniels, A. D.; Strain, M. C.; Farkas, O.; Malick, D. K.; Rabuck, A. D.; Raghavachari, K.; Foresman, J. B.; Ortiz, J. V.; Cui, Q.; Baboul, A. G.; Clifford, S.; Cioslowski, J.; Stefanov, B. B.; Liu, G.; Liashenko, A.; Piskorz, P.; Komaromi, I.; Martin, R. L.; Fox, D. J.; Keith, T.; Al-Laham, M. A.; Peng, C. Y.; Nanayakkara, A.; Challacombe, M.; Gill, P. M. W.; Johnson, B.; Chen, W.; Wong, M. W.; Gonzalez, C.; Pople, J. A. *Gaussian03*; Revision D.01 ed.; Gaussian, Inc.: Wallingford, CT, 2004.
(38) Schlegel, H. B. *J. Comput. Chem.* **1982**, *3*, 214.
(39) Ahlrichs, R.; Bar, M.; Haser, M.; Horn, H.; Kolmel, C. *Chem. Phys. Lett.* **1989**, *162*, 165.
(40) Weigend, F.; Ahlrichs, R. *Phys. Chem. Chem. Phys.* **2005**, *7*, 3297.
(41) Dunning, T. H. *J. Chem. Phys.* **1989**, *90*, 1007.
(42) Kendall, R. A.; Dunning, T. H.; Harrison, R. J. *J. Chem. Phys.* **1992**, *96*, 6796.
(43) Knizia, G.; Adler, T. B.; Werner, H. J. *J. Chem. Phys.* **2009**, *130*, 054104.
(44) Peterson, K. A.; Puzzarini, C. *Theor. Chem. Acc.* **2005**, *114*, 283.
(45) Peterson, K. A.; Adler, T. B.; Werner, H. J. *J. Chem. Phys.* **2008**, *128*, 084102.

(46) Werner, H. J.; Knowles, P. J.; Lindh, R.; Manby, F. R.; Schütz, M. http://www.molpro.net, 2009.
(47) Eichkorn, K.; Treutler, O.; Ohm, H.; Häser, M.; Ahlrichs, R. *Chem. Phys. Lett.* **1995**, *240*, 283.
(48) Weigend, F. *Phys. Chem. Chem. Phys.* **2006**, *8*, 1057.
(49) Weigend, F.; Haser, M.; Patzelt, H.; Ahlrichs, R. *Chem. Phys. Lett.* **1998**, *294*, 143.
(50) Schütz, M.; Manby, F. R. *Phys. Chem. Chem. Phys.* **2003**, *5*, 3349.
(51) Manby, F. R.; Knowles, P. J.; Lloyd, A. W. *J. Chem. Phys.* **2001**, *115*, 9144.
(52) Momma, K.; Izumi, F. *J. Appl. Crystallogr.* **2008**, *41*, 653.
(53) Laaksonen, L. *J. Mol. Graph.* **1992**, *10*, 33.
(54) Barone, V. *J. Chem. Phys.* **2004**, *120*, 3059.
(55) Clabo, D. A.; Allen, W. D.; Remington, R. B.; Yamaguchi, Y.; Schaefer, H. F. *Chem. Phys.* **1988**, *123*, 187.
(56) Barone, V. *Chem. Phys. Lett.* **2004**, *383*, 528.
(57) Carbonniere, P.; Lucca, T.; Pouchan, C.; Rega, N.; Barone, V. *J. Comput. Chem.* **2005**, *26*, 384.
(58) Barone, V. *J. Chem. Phys.* **2005**, *122*, 014108.
(59) Valle, J. J.; Eyler, J. R.; Oomens, J.; Moore, D. T.; van der Meer, A. F. G.; von Helden, G.; Meijer, G.; Hendrickson, C. L.; Marshall, A. G.; Blakney, G. T. *Rev. Sci. Instrum.* **2005**, 76.
(60) Oepts, D.; van der Meer, A. F. G.; van Amersfoort, P. W. *Infrared Phys. Technol.* **1995**, *36*, 297.
(61) Sundholm, D.; Tokman, M.; Pyykkö, P.; Eliav, E.; Kaldor, U. *J. Phys. B-At. Mol. Opt. Phys.* **1999**, *32*, 5853.
(62) Cook, D. B. *Mol. Phys.* **1981**, *42*, 235.
(63) Neogrady, P.; Kellö, V.; Urban, M.; Sadlej, A. J. *Int. J. Quantum Chem.* **1997**, *63*, 557.
(64) Baker, J. *Chem. Phys. Lett.* **1988**, *152*, 227.
(65) Schwerdtfeger, P.; Ischtwan, J. *J. Mol. Struct. (THEOCHEM)* **1994**, *112*, 9.
(66) Forsberg, B.; He, Z.; He, Y.; Cremer, D. *Int. J. Quantum Chem.* **2000**, *76*, 306.
(67) Botschwina, P.; Oswald, R. *J. Phys. Chem. A* **2010**, *114*, 4875.
(68) Gutsev, G. L.; Bartlett, R. J.; Compton, R. N. *J. Chem. Phys.* **1998**, *108*, 6756.
(69) Schröder, D.; Schalley, C. A.; Harvey, J. N.; Schwarz, H. *Int. J. Mass Spectrom.* **1999**, *187*, 25.
(70) Ard, S.; Mirsaleh-Kohan, N.; Steill, J. D.; Oomens, J.; Nielsen, S. B.; Compton, R. N. *J. Chem. Phys.* **2010**, *132*, 094301.
(71) Hoffmann, M.; Grajewski, J.; Gawronski, J. *New J. Chem.* **2010**, *34*, 2020.
(72) Oomens, J.; Steill, J. D. *J. Phys. Chem. A* **2008**, *112*, 3281.
(73) Spinner, E. *J. Chem. Soc. B-Phys. Org.* **1967**, 874.